Linear Multiselenium Interactions in Dicationic Oligomers of 1,5-(Diselena)canes: Behavior of Se_{m_c} $\sigma(m_c\text{c-}n_e\text{e})$ $(6 \leq m_c \leq 16)$ Elucidated with QTAIM Dual Functional Analysis

Satoko Hayashi,* Taro Nishide, Kengo Nagata, and Waro Nakanishi*[a]

The intrinsic dynamic and static nature m_c center-n_e electron interactions of the σ-type $\sigma(m_c\text{c-}n_e\text{e})$ were elucidated for the Se-Se interactions in dicationic oligomers of $\mathrm{Se(CH_2CH_2CH_2)_2Se}$ (**1** (Se, Se)) [n^{2+} (Se, Se): $n = 1–8$], especially for $m_c \geq 6$, where n^{2+} (Se, Se: $n = 1–8$) are abbreviated by n^{2+} ($n = 1–8$), respectively. QTAIM dual functional analysis (QTAIM-DFA) was applied to the interactions. Perturbed structures generated using coordinates derived from the compliance constants (C_{ii}) were employed for QTAIM-DFA. Each Se-*-Se in **1^{2+}** and **2^{2+}** has the nature of CT-TBP (trigonal bipyramidal adduct formation through CT) and Cov-w (weak covalent), respectively, which supply the starting points of the investigations. The asterisk emphasizes the existence of a bond critical point on the interaction. All Se-*-Se in **3^{2+}** are classified by the regular closed shell (*r*-CS) interactions and characterized as CT-MC (molecular complex formation through CT), which are denoted as *r*-CS/CT-MC, except for the central interaction, of which nature is *r*-CS/CT-TBP. Most interactions in **4^{2+}**–**8^{2+}** are *r*-CS/*t*-HB_wc (typical-HB with covalency) but some are *pure*-CS/*t*-HB_nc (*t*-HB with no covalency). The linear $\mathrm{Se_{2n}}^{2+}$ interactions in **2^{2+}**–**8^{2+}** seem close to those without any limitations, since the nature of Se-*-Se inside and outside of $\mathrm{(CH_2CH_2CH_2)_2}$ are very similar with each other. The linear $\mathrm{Se_{2n}}^{2+}$ interactions in **3^{2+}**–**8^{2+}** are shown to be analyzed as $\sigma(m_c\text{c-}n_e\text{e}: 6 \leq m_c \leq 16)$, not by the accumulated σ(3c–4e).

1. Introduction

We have proposed the concept of "extended hypervalent bonds/interactions of the σ-type, $\sigma(m_c\text{c-}n_e\text{e})$ (m_c center-n_e electron interactions: $m_c \geq 4$; $m_c < n_e < 2m_c$),[1–3] for the linear interactions between atoms of the main group elements[4] longer than three, after hypervalent bonds/interactions of σ(3c–4e).[2,4] The chemistry of σ(4c–6e) has been developed through the preparation of the compounds containing σ(4c–6e) and the structural determinations by the X-ray crystallographic analysis. The linear alignment of four chalcogen atoms ($E_2E'_2$) at the naphthalene 1,8-positions of 1-(8-PhE'C$_{10}$H$_6$)EE(C$_{10}$H$_6$E'Ph-8')-1' are the typical example for $E_2E'_2$ σ(4c–6e), where E, E' = S and Se.[1] $E_2E'_2$ σ(4c–6e) are characterized by the charge transfer (CT) of the $n_p(E') \rightarrow \sigma^*(E\text{-}E) \leftarrow n_p(E')$ type, where $n_p(E')$ and $\sigma^*(E\text{-}E)$ stand for the p-type lone pair orbitals of E' and σ*-orbital of E-E, respectively. E_2X_2 σ(4c–6e)[5] and X_4 σ(4c–6e)[6] show similar trend in the interactions. It is strongly suggested for σ(4c–6e) to play an important role not only in the development of high

functionalities in materials but also in the key processes of biological and pharmaceutical activities, recently.[7] The C_2E_2O (5c–6e) interactions (E = Se and S) are also successfully detected in 1,8-bis(phenylselanyl/thio)anthraquinones and 9-methoxy-1,8-bis(phenylselanyl/thio)anthracenes.[1d,8]

It is challenging to clarify the nature of $\sigma(m_c\text{c-}n_e\text{e}: m_c \geq 6)$. Each $\sigma(m_c\text{c-}n_e\text{e}: m_c \geq 6)$ consists of σ-type linear MOs of $\psi_1 - \psi_{mc}$, where ψ_i ($1 \leq i \leq m_c$) has the nodal planes (n_{np}) of $i-1$. Figure 1 illustrates the approximate MO model, exemplified by E_{10} σ(10c–18e). MOs in E_{10} σ(10c–18e) consist of $\psi_1 - \psi_{10}$, which contain n_{np} of 0–9, respectively. Dicationic oligomers of 1,5-(dichalcogena)canes [E(CH$_2$CH$_2$CH$_2$)$_2$E': **1** (E, E'), where E, E' = S, Se, and Te] seem an excellent candidate to supply $\sigma(m_c\text{c-}n_e\text{e}: m_c \geq 6; m_c < n_e < 2m_c)$. Research groups of Furukawa[9] and
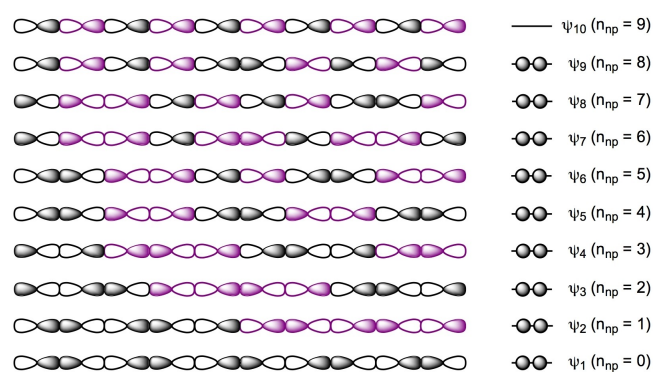

Figure 1. Approximate MO model for E_{10} σ(10c–18e). Colors correspond to the relative signs of AOs.
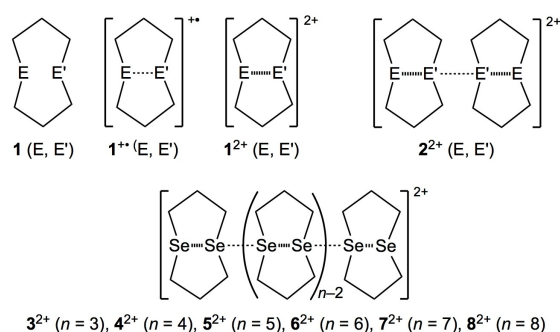
[a] Dr. S. Hayashi, T. Nishide, K. Nagata, Prof. W. Nakanishi
Faculty of Systems Engineering, Wakayama University
930 Sakaedani, Wakayama 640-8510 (Japan)
E-mail: hayashi3@sys.wakayama-u.ac.jp
nakanisi@sys.wakayama-u.ac.jp

ChemistryOpen

Full Papers
doi.org/10.1002/open.202100017

Chemistry Europe
European Chemical
Societies Publishing

Glass[10] have investigated the chemistry of **1** (E, E′) and the dimers, energetically. The transannular interactions are the important issue in the chemistry.[11] Two-electron oxidation of neural monomers **1** (E, E′) will give the corresponding dicationic monomers **1**$^{2+}$ (E, E′), via the corresponding radical cationic monomers **1**$^{•+}$ (E, E′), formed through the one-electron oxidation of **1** (E, E′). Dicationic dimers **2**$^{2+}$ (E, E′) will form in the reaction of **1**$^{2+}$ (E, E′) with **1** (E, E′) and/or the dimerization of **1**$^{•+}$ (E, E′). Scheme 1 illustrates n^{2+} (E, E′: $n = 1–8$), together with **1** (E, E′) and **1**$^{•+}$ (E, E′), where (E, E′) = (S, S), (S, Se), (S, Te), (Se, Se), (Se, Te) and (Te, Te), while $n*$ (Se, Se: $n = 1–8$; = **null, ·+, and 2+) are abbreviated by n**, respectively. Structures, determined by the X-ray crystallographic analysis, have been reported for [S(CH$_2$CH$_2$CH$_2$)$_2$S]$^{2+}$ [**1**$^{2+}$ (S, S)],[12] [S-(CH$_2$CH$_2$CH$_2$)$_2$Se]$^{2+}$ [**1**$^{2+}$ (S, Se)],[13] [S(CH$_2$CH$_2$CH$_2$)$_2$Te]$^{2+}$ [**1**$^{2+}$ (S, Te)],[13] [Se(CH$_2$CH$_2$CH$_2$)$_2$Se]$^{2+}$ (**1**$^{2+}$),[14] [S(CH$_2$CH$_2$CH$_2$)SeSe(CH$_2$CH$_2$CH$_2$)$_2$S]$^{2+}$ [**2**$^{2+}$ (S, Se)],[15] and [Se(CH$_2$CH$_2$CH$_2$)$_2$SeSe(CH$_2$CH$_2$CH$_2$)$_2$Se]$^{2+}$ (**2**$^{2+}$).[16,17] σ(4c–6e) serves as the backbone of **2**$^{2+}$ (S/Se, Se), together with σ(2c–2e) of **1**$^{2+}$ (S/Se, Se).[18] Scheme 2 explains the notation for the chalcogen atoms and the interactions in n^{2+} ($n = 1–8$), where the numberings start at the central positions.

We have reported the nature of the chalcogen-chalcogen interactions in **2**$^{•+}$ (E, E′) and **2**$^{2+}$ (E, E′),[18] together with that in **1** (E, E′), **1**$^{•+}$ (E, E′), and **1**$^{2+}$ (E, E′).[18] The radical cationic dimers **2**$^{•+}$ (E, E′) and dicationic dimers **2**$^{2+}$ (E, E′) are shown to be stable, and the interactions are well clarified with the QTAIM approach. Are the higher dicationic oligomers of **1** [n^{2+} (E, E′:
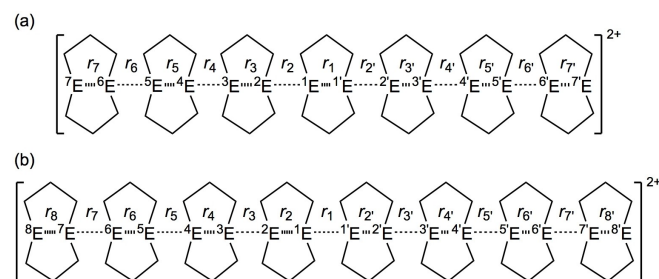
$3 \leq n \leq 8$)] stable? What is the nature of the chalcogen-chalcogen interactions in n^{2+} (E, E′: $3 \leq n \leq 8$)? The nature of the chalcogen-chalcogen interactions in n^{2+} (E, E′: $3 \leq n \leq 8$) is to be elucidated, with the structural feature and the stability.

QTAIM dual functional analysis (QTAIM-DFA),[19] which we proposed based on the QTAIM approach introduced by Bader,[20] is employed to elucidate the nature. The charge density ($\rho(r)$) at a bond critical point (BCP, *[20]) on the bond path (BP) is denoted by $\rho_b(r_c)$ in this paper, as are other QTAIM functions such as the total electron energy densities $H_b(r_c)$, potential energy densities $V_b(r_c)$, and kinetic energy densities $G_b(r_c)$ at BCPs.[20] $H_b(r_c)$ are plotted versus $H_b(r_c) - V_b(r_c)/2$ ($= (\hbar^2/8m)\nabla^2\rho_b(r_c)$; see eq (SA2) in the Supporting Information) in QTAIM-DFA. In our treatment, data from the perturbed structures around the fully optimized structures are employed, in addition to those from the fully optimized ones. Data from the fully optimized structures in the plots are analyzed using the polar coordinate (R, θ) representation, which corresponds to the static nature of the interactions.[19] Each interaction plot for the data from both the perturbed and fully optimized structures is expressed by (θ_p, κ_p), where θ_p corresponds to the tangent line and κ_p is the curvature of the plot. θ and θ_p are measured from the y-axis and the y-direction, respectively. (See also Figure 7 for the definition of QTAIM-DFA parameters of (R, θ) and (θ_p, κ_p), drawn exemplified by ^{1}Se-*-^{2}Se of **5**$^{2+}$.) The concept of the dynamic nature of interactions has been proposed based on (θ_p, κ_p).[21]

The perturbed structures necessary for QTAIM-DFA are generated with CIV (QTAIM-DFA with CIV), which we proposed recently.[22] The coordinates corresponding to the compliance constants C_{ii} for the internal vibrations are employed in CIV.[23–26] CIV is shown to be a highly reliable method to generate the perturbed structures. The dynamic nature of interactions based on the perturbed structures with CIV is described as the "intrinsic dynamic nature of interactions" since the coordinates are invariant to the choice of coordinate system. QTAIM-DFA with CIV is applied to standard interactions and rough criteria that distinguish the interaction in question from others that are obtained. QTAIM-DFA and the criteria are explained in the Appendix of the Supporting Information using Schemes SA1–SA3, Figures SA1 and SA2, Table SA1, and eqs (SA1)–(SA7). The basic concept of the QTAIM approach is also explained.

Theoretical investigations on the phenomena arising from σ(m_cc-n_ee: $m_c \geq 4$) seem successively increasing.[1,2,27–29] However, it is still of high importance to clarify the causality in the phenomena from which the interactions arise, with physical necessity. Indeed, the knowledge of the behavior of σ(4c–6e) and σ(5c–6e) has increased, but the nature of σ(m_cc-n_ee: $m_c \geq 6$) seems still to be in the dark, while the alignments of multi-chalcogen atoms are often observed in crystals. We elucidated the intrinsic dynamic and static nature of each Se-*-Se in σ(m_cc-n_ee: $6 \leq m_c \leq 16$) in n^{2+} ($3 \leq n \leq 8$), by QTAIM-DFA with CIV. Each Se-*-Se in n^{2+} ($3 \leq n \leq 8$) is classified and characterized employing the criteria as a reference. The nature of each Se-*-Se in σ(m_cc-n_ee: $6 \leq m_c \leq 16$) of n^{2+} ($3 \leq n \leq 8$) is discussed in a unified form, together with those for **1**$^{2+}$ and **2**$^{2+}$, as the starting points

Scheme 1. Dicationic oligomers n^{2+} (E, E′: $n = 1–8$) of 1,5-(dichalcogena) canes [**1** (E, E′)], together with **1** (E, E′) and the radical cations **1**$^{•+}$ (E, E′), where $n*$ (Se, Se: $n = 1–8$; = null, ·+, and 2+) are abbreviated by n, respectively.

Scheme 2. Notation of E and E–E (E = Se) in n^{2+}, exemplified by **7**$^{2+}$ for n of odd (a) and **8**$^{2+}$ for n of even (b). (Numbering starting from the central positions.)

ChemistryOpen

Full Papers
doi.org/10.1002/open.202100017

Chemistry Europe
European Chemical
Societies Publishing

for n^{2+} ($3 \leq n \leq 8$). The structural feature and the stability are also discussed.

Computational Methods

Calculations were performed employing the Gaussian 09 program package.[30] The 6–311G(3d) basis set was employed for Se with the 6–311G(d) basis set for C and H at the DFT level of M06-2X.[31] The basis set system is called BSS-A (M06-2X/BSS-A), in this paper. To examine the basis set and level dependence on the nature, MP2[32]/BSS-B was also applied to **1** and **1**$^{2+}$ and M06-2X/BSS-B to **2**$^{2+}$, where the 6–311+G(3df) basis set was employed for Se with the 6–311+G(d,p) basis set for C and H in BSS-B. The optimized structures were confirmed by the frequency analysis. The results of the frequency analysis are used to obtain the compliance constants (C_{ii}) and the coordinates corresponding to C_{ii} (C_i). NBO analysis[33] was applied under M06-2X/BSS-A.

The method to generate the perturbed structures with CIV is explained in eq (1). The ith perturbed structure in question (S_{iw}) is generated by the addition of the ith coordinates derived from C_{ii} (C_i) to the standard orientation of a fully optimized structure (S_o) in the matrix representation. The coefficient g_{iw} in eq (1) controls the structural difference between S_{iw} and S_o: g_{iw} is determined to satisfy eq (2) for r, where r and r_o stand for the interaction distances in question in the perturbed and fully optimized structures, respectively, with $a_o = 0.52918$ Å (Bohr radius). The C_i values of five digits are used to predict S_{iw}.

$$S_{iw} = S_o + g_{iw} \cdot C_1 \tag{1}$$

$$r = r_o + w a_o$$
$$(w = (0), \pm 0.025, \text{ and } \pm 0.05; a_o = 0.52918 \text{ Å}) \tag{2}$$

$$y = c_o + c_1 x + c_2 x^2 + c_3 x^3$$
$$(R_c^2 : \text{ square of correlation coefficient}) \tag{3}$$

QTAIM functions were calculated using the same basis set system as in the optimizations, unless otherwise noted, and were analyzed with the AIM2000[34] and AIMAll[35] programs. The $H_b(r_c)$ values are plotted versus $H_b(r_c) - V_b(r_c)/2$ for five data points of $w = 0, \pm 0.025$, and ± 0.05 in eq (2) in QTAIM-DFA. Each plot is analyzed using a regression curve of the cubic function, shown in eq (3), where (x, y) = ($H_b(r_c) - V_b(r_c)/2$, $H_b(r_c)$) ($R_c^2 > 0.99999$ in usual).[19e]

2. Results and Discussion

2.1. Structural Feature of n^{2+} ($n = 1$–8: $E = E' = Se$)

The structures of n^{2+} ($n = 3$–8) were optimized with M06-2X/BSS-A, retaining the C_2 or higher symmetry, together with **1**, **1**$^{2+}$ and **2**$^{2+}$. The optimized structures are not shown in figures but some of them can be found in molecular graphs drawn on the optimized structures (see Figure 6 and Figure S1 of the Supporting Information). The Se-Se distances in the optimized structures of n^{2+} ($n = 1$–8) are collected in Table S1 of the Supporting Information. Charges developed on the Se atoms (Qn(Se)) are calculated for the optimized structures of n^{2+} ($n = 1$–8), employing the natural population analysis (NPA). The Qn(Se) values are summarized in Table S2 of the Supporting

Information. Energies for the formation of n^{2+} ($n = 2$–8) from the components ($1^{2+} + (n-1) \cdot 1$) [$\Delta E(n^{2+}) = E(n^{2+}) - (E(1^{2+}) + (n-1)E(1))$] are also calculated. The $\Delta E(n^{2+})$ values are given in Table S3 of the Supporting Information.

What is the behavior of r(Se, Se) in 3^{2+}–8^{2+}? Figure 2 shows the plot of each r(Se, Se) values for 3^{2+}–8^{2+}, together with **1**, **1**$^{2+}$ and **2**$^{2+}$, collected in Table S1 of the Supporting Information. While all r(Se, Se) values in 3^{2+}–8^{2+} and 2^{2+} are longer than the value of **1**$^{2+}$, they are shorter than the value of **1**, except for r(^{1}Se, ^{1}Se) in 6^{2+}, r(^{1}Se, ^{2}Se) in 7^{2+}, and r(^{1}Se, ^{1}Se) and r(^{2}Se, ^{3}Se) in 8^{2+}. The central r(^{1}Se, ^{1}Se) distances become longer in the order of ($1^{2+} < 2^{2+} <$) $3^{2+} < 4^{2+} < 5^{2+} < 7^{2+}$ ($<$ **1**) $< 6^{2+} < 8^{2+}$. The distance becomes longer if it goes more outside in 2^{2+}–4^{2+}, whereas the zig-zag type behavior is predicted for r(Se, Se) in 5^{2+}–8^{2+}. While r(^{3}Se, ^{4}Se) is longest for 5^{2+}, r(^{1}Se, ^{2}Se) is longest for 7^{2+} and the r(^{1}Se, ^{1}Se) values are longest for 6^{2+} and 8^{2+}. The behavior for 5^{2+} and 7^{2+} seems intermediate between the two groups. In 6^{2+}–8^{2+}, some r(Se, Se) distances at approximately the central positions are longer than that of **1**, while the distances of five most outside positions in 6^{2+}–8^{2+} are shorter than that of **1**. These results may suggest that the linear Se-Se interactions in 6^{2+}–8^{2+} can be analyzed separated by the three parts, two outside parts and a remaining central one. The behavior of the central part seems very complex for 6^{2+}–8^{2+}.

What factors operate to stabilize the Se-Se interactions in 3^{2+}–8^{2+}, together with **1**, **1**$^{2+}$ and **2**$^{2+}$? Two electron removal from **1** forms the stable Se$_2$ σ(2c–2e) of **1**$^{2+}$, as discussed above. The positive charges developed at the Se atoms calculated with NPA (Qn(Se)) are analyzed, next. Figure 3 shows the plot of Qn(Se) for 3^{2+}–8^{2+}, together with **1**, **1**$^{2+}$ and **2**$^{2+}$, which are collected in Table S2 of the Supporting Information (see Scheme 2 for the notation of the Se atoms). All Qn(Se) values for 2^{2+}–8^{2+} are larger than the value of **1** but smaller than that of **1**$^{2+}$. Qn(Se) shows a characteristic behavior depending on the lengths of the alignments, n in n^{2+}. The values are largest at the central Se atoms and become smaller if the Se atom goes to more outside positions from the central position(s) for 2^{2+}–5^{2+}, although the trend is not so sharp around the central positions in 5^{2+}. However, Qn(Se) values are smallest at the central

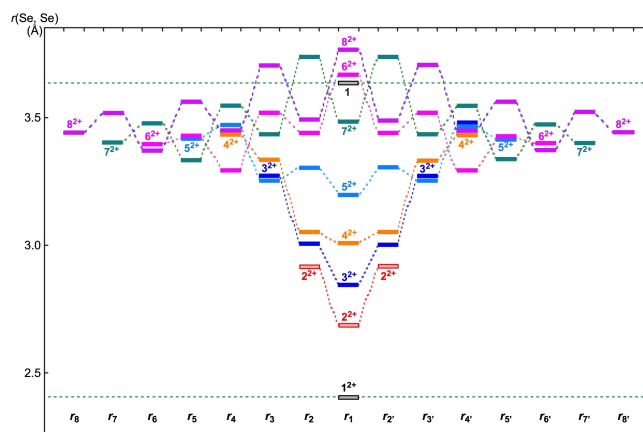**Figure 2.** Plots of each r(Se, Se) for 3^{2+}–8^{2+}, together with **1**, **1**$^{2+}$, and **2**$^{2+}$.

ChemistryOpen

Full Papers
doi.org/10.1002/open.202100017

Chemistry Europe
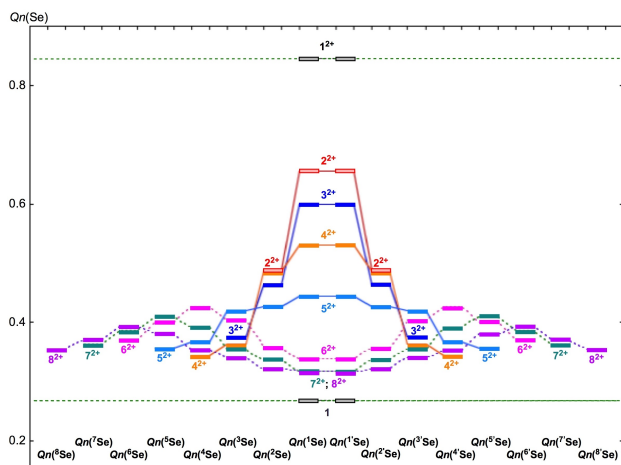European Chemical
Societies Publishing

Figure 3. Plots of each Qn(Se) for 3^{2+}–8^{2+}, together with **1**, 1^{2+}, and 2^{2+}.

position, and the values become larger, then reach to maximum and then decrease again, as the Se atom goes to more outside positions from the central position(s) for 6^{2+}–8^{2+}. The results may also suggest that it is better to analyze the interactions separately as the three parts for 6^{2+}–8^{2+}. Nevertheless, the energy lowering effect in the formation of 6^{2+}–8^{2+} seems not so different from the effect in the formation of 3^{2+}–5^{2+}, if the effect per component is compared, as a whole (see, Figure 5).

How are the Se-Se distances correlated to Qn(Se)? The Se-Se interaction seems stronger, as the Se atoms at both sides of the interaction are more positively charged. Namely, the $r(^{u}\text{Se}, {}^{v}\text{Se})$ values for ^{u}Se-^{v}Se are expected to be linearly correlated to $(Qn(^{u}\text{Se}) + Qn(^{v}\text{Se}))$. The $r(^{u}\text{Se}, {}^{v}\text{Se})$ values in Table S1 of the Supporting Information are plotted versus $(Qn(^{u}\text{Se}) + Qn(^{v}\text{Se}))$ in Table S2 of the Supporting Information, evaluated with M06-2X/BSS-A. Figure 4 shows the plot, which gives very good correlations if it is analyzed as two correlations. The two groups
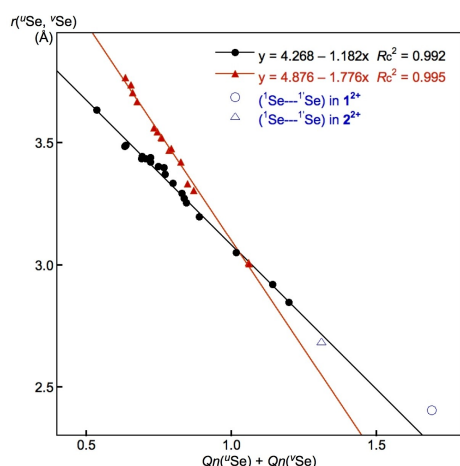
(G(**B**) and G(**R**)) are shown by black circles and red triangles, respectively, in the plot. They give very good correlations ($y = -1.182x + 4.268$ ($R_c^2 = 0.992$) for G(**B**) and $y = -1.776x + 4.876$ ($R_c^2 = 0.995$) for G(**R**)), although the data points for (^{1}Se, $^{1'}\text{Se}$) of 1^{2+} and 2^{2+} are omitted from the correlations, which are shown in blue. The colors in the plot of Figure 4 are the same as those for the r(Se, Se) values in Table S1 of the Supporting Information, respectively. Data from (^{u}Se, ^{v}Se) belong to G(**B**) if (^{u}Se, ^{v}Se) are contained in the cyclic $^{u}\text{Se}(CH_2CH_2CH_2)_2{}^{v}\text{Se}$ system, except for those in 1^{2+}.

However, data from (^{u}Se, ^{v}Se) form G(**R**) if (^{u}Se, ^{v}Se) belong to the adjacent two cyclic $Se(CH_2CH_2CH_2)_2Se$ systems, except for those in 2^{2+}. The results show that $r(^{u}\text{Se}, {}^{v}\text{Se})$ becomes shortened proportionally to the increase in $Qn(^{u}\text{Se}) + Qn(^{v}\text{Se})$. Namely, the ^{u}Se-^{v}Se interaction becomes stronger as $Qn(^{u}\text{Se}) + Qn(^{v}\text{Se})$ increases, irrespective of the increase of the electrostatic repulsion between ^{u}Se and ^{v}Se, which must weaken the interaction. Data for 1^{2+} and 2^{2+} slightly deviate from the correlations, maybe due to the highly strong nature of the ^{1}Se-$^{1'}\text{Se}$ interactions. The results should correlate well with the ΔE values discussed below.

What is the behavior of the relative energies ΔE in the formation of n^{2+} ($n = 3$–8) from the components? Figure 5 shows the plot of ΔE (n^{2+}) versus n of n^{2+} ($n = 3$–8), evaluated with M06-2X/BSS-A, together with ΔE (2^{2+}). The ΔE value of 3^{2+} is -3.60 eV, the magnitude of which is larger than that of 2^{2+} by 0.79 eV. While 2^{2+} is stabilized by only one molecules of **1**, 1^{2+} in 3^{2+} is stabilized by two molecules of **1**. However, the magnitude of ΔE per the component in 3^{2+} (-1.20 eV $= -3.60$ eV/3) is smaller than that of $\Delta 2^{2+}$ (-1.41 eV $= -2.81$ eV/2). The magnitudes of $\Delta\Delta E$ (n^{2+}) $[= E(n^{2+}) - \Delta E((n-1)^{2+})]$ increase almost constantly by approximately 0.38 eV, when they go from 3^{2+} to 8^{2+}. The results show that the dicationic trimmer 3^{2+} is well stabilized and so are the higher oligomers, 4^{2+}–8^{2+}.

After clarification of the structural feature of 1^{2+}–8^{2+}, the next extension is to elucidate the nature of the Se-*-Se interactions, by applying QTAIM-DFA.
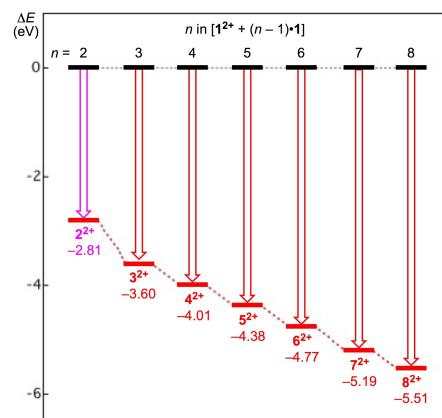

Figure 4. Plots of $r(^{u}\text{Se}, {}^{v}\text{Se})$ versus $(Qn(^{u}\text{Se}) + Qn(^{v}\text{Se}))$ in 3^{2+}–8^{2+}, evaluated with M06-2X/BSS-A. Data from G(**B**) are shown by black circles for the inside Se-Se interactions in $^{u}\text{Se}(CH_2CH_2CH_2)_2{}^{v}\text{Se}$. Data from G(**R**) are shown by red triangles if (^{u}Se, ^{v}Se) belong to the outside ones. Data from 1^{2+} and 2^{2+} are also shown by the hollow blue cycle and triangle, respectively.

Figure 5. Energies for the formation of n^{2+} from $[1^{2+} + (n-1)\cdot \textbf{1}]$ ($n = 3$–8 and 2), evaluated with M06-2X/BSS-A.

ChemistryOpen

Full Papers
doi.org/10.1002/open.202100017

**Chemistry
Europe**
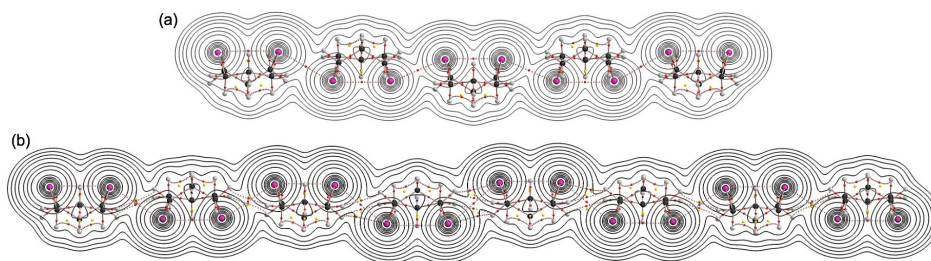European Chemical
Societies Publishing

Figure 6. Molecular graphs with contour maps of $\rho_b(r_c)$ drawn on the, where all selenium atoms are located, plane for 5^{2+} (a) and 8^{2+} (b), calculated with M06-2X/BSS-A.

2.2. Molecular Graphs with Contour Plots around Se-*-Se

Figure 6 shows the molecular graphs with contour plots of 5^{2+} and 8^{2+}, for example. All BCPs expected are detected, including the CPs between the Se-Se atoms and those for very weak interactions in the components and those between them. BCPs between Se atoms appear at the (three-dimensional) saddle points of $\rho(r)$. The BCPs for 2^{2+}–7^{2+}, other than 5^{2+}, are drawn in Figure S1 of the Supporting Information. All BCPs expected for the Se-Se interactions are detected.

2.3. Survey of ^{u}Se-*-^{v}Se in n^{2+} ($n = 1$–8)

BPs, corresponding to Se-*-Se, seem straight, as shown in Figure 6 and Figure S1 of the Supporting Information. To examine the linearity of the BPs further, the lengths of the BPs (r_{BP}) in question are calculated for all Se-*-Se of n^{2+} ($n = 1$–8), together with the corresponding straight-line distances (R_{SL}). The values are collected in Table S1 of the Supporting Information, together with the differences between them ($\Delta r_{BP} = r_{BP} - R_{SL}$).

The Δr_{BP} values are less than 0.04 Å. As a result, BPs corresponding to all Se-*-Se of n^{2+} ($n = 1$–8) can be approximated as the straight lines (see also Figure S2 of the Supporting Information).

QTAIM functions are calculated for 1^{2+}–8^{2+} at BCPs on Se-*-Se with M06-2X/BSS-A. Table 1 collects the $\rho_b(r_c)$, $H_b(r_c) - V_b(r_c)/2$, and $H_b(r_c)$ values. Figure 7 shows the plots of $H_b(r_c)$ versus $H_b(r_c) - V_b(r_c)/2$ for each Se-*-Se, exemplified by 5^{2+}. (See Figure S3 of the Supporting Information for 6^{2+} and 7^{2+}.) All data for the optimized structures appear in the *regular* CS region, showing the CT nature of the interactions. The plots are analyzed according to eqs (SA3)–(SA6) of the Supporting Information. Table 1 collects the QTAIM-DFA parameters of (R, θ) and (θ_p, κ_p) for each Se-*-Se of 3^{2+}–8^{2+}, 1, 1^{2+} and 2^{2+}, together with the C_{ii} values corresponding to the interactions in question. The (θ_p, κ_p) values, evaluated with CIV, should be denoted by ($\theta_{p:CIV}$, $\kappa_{p:CIV}$), respectively. However, (θ_p, κ_p) will be used in place of ($\theta_{p:CIV}$, $\kappa_{p:CIV}$) to simplify the notation.
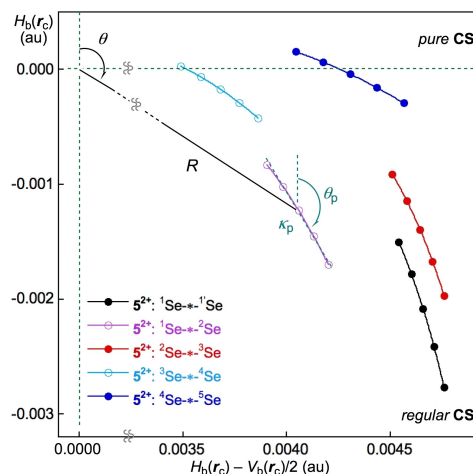

Figure 7. Plots of $H_b(r_c)$ versus $H_b(r_c) - V_b(r_c)/2$ for Se-*-Se in 5^{2+}.

2.4. Nature of each Se-*-Se in n^{2+} ($n = 1$–8)

The central ^{1}Se-*-$^{1'}$Se interaction is strongest in 3^{2+}–5^{2+} and 2^{2+}, among the interactions in the same species. The strength of ^{1}Se-*-$^{1'}$Se becomes weaker in the order of ($1^{2+} > 2^{2+} >$) $3^{2+} > 4^{2+} > 5^{2+}$. The ^{u}Se-*-^{v}Se interaction in the same species becomes weaker, if it goes from the central position to a more outside position, namely, ^{1}Se-*-$^{1'}$Se $> ^1$Se-*-^{2}Se $> ^2$Se-*-^{3}Se $> ^3$Se-*-^{4}Se $> ^4$Se-*-^{5}Se for 3^{2+}–5^{2+} and/or 2^{2+}, although the order changes as in ^{2}Se-*-^{3}Se $> ^1$Se-*-^{2}Se for 5^{2+}. However, ^{1}Se-*-$^{1'}$Se is weakest for 6^{2+} and 8^{2+}, while ^{1}Se-*-^{2}Se is weaker than ^{2}Se-*-^{3}Se for 7^{2+}. The strength of ^{u}Se-*-^{v}Se shows ripple-like changes from the center to the outside for 6^{2+}–8^{2+}. The behavior of ^{u}Se-*-^{v}Se of 5^{2+} seems intermediate between the two groups of 3^{2+}–4^{2+} and 6^{2+}–8^{2+}. The ^{1}Se-*-$^{1'}$Se interaction is strongest in 5^{2+} but the strength of ^{u}Se-*-^{v}Se waves slightly from the central position to a more outside position. The behavior of Se-*-Se detected by the QTAIM parameters should be closely related to the behavior of r(Se, Se), although there seem to be some differences in the magnitudes (see Figure 2).

Before a detailed discussion of the nature, it is instructive to survey the criteria shown in Scheme SA3 and Table SA1 of the Supporting Information. While θ classifies the interactions, θ_p characterizes them. The criteria tell us that $45° < \theta < 180°$ ($0 < H_b(r_c) - V_b(r_c)/2$) for the closed shell (CS) interactions and $180° < \theta < 226.6°$ ($H_b(r_c) - V_b(r_c)/2 < 0$) for the shard shell (SS)

Table 1. QTAIM Functions and QTAIM-DFA Parameters Evaluated for the Dicationic Oligomers of *Cyclo*-1,5-Se(CH$_2$CH$_2$CH$_2$)$_2$Se (**1**), **3**$^{2+}$–**8**$^{2+}$, **1**$^{2+}$, and **2**$^{2+}$, together with **1**, Employing the Perturbed Structures Generated with CIV.[a,b]

Species ^{u}Se-*-^{v}Se	$\rho_b(r_c)$ [ea_o^{-3}]	$c\nabla^2\rho_b(r_c)$[c] [au]	$H_b(r_c)$ [au]	R[d] [au]	θ [e] [°]	C_{ii}[f] [Å mdyn^{-1}]	θ_p[g] [°]	κ_p[h] [au^{-1}]	Predicted Nature
3^{2+}									
^{1}Se-*-^{1}'Se	0.0489	0.0036	−0.0099	0.0105	159.7	2.08	183.4	28.3	*r*-CS/CT-TBP
^{1}Se-*-^{2}Se	0.0379	0.0043	−0.0053	0.0069	141.0	4.41	177.1	60.8	*r*-CS/CT-MC
^{2}Se-*-^{3}Se	0.0220	0.0047	−0.0010	0.0048	101.9	4.48	151.9	203	*r*-CS/CT-MC
4^{2+}									
^{1}Se-*-^{1}'Se	0.0380	0.0042	−0.0054	0.0068	142.0	5.46	178.8	32.2	*r*-CS/CT-MC
^{1}Se-*-^{2}Se	0.0342	0.0046	−0.0044	0.0064	133.5	3.35	175.5	48.9	*r*-CS/CT-MC
^{2}Se-*-^{3}Se	0.0218	0.0040	−0.0010	0.0042	103.5	10.69	153.6	181	*r*-CS/CT-MC
^{3}Se-*-^{4}Se	0.0163	0.0042	0.0000	0.0042	90.0	4.40	128.4	396	*p*-CS/*t*-HB$_{nc}$
5^{2+}									
^{1}Se-*-^{1}'Se	0.0262	0.0047	−0.0021	0.0051	114.1	4.86	170.2	85.3	*r*-CS/CT-MC
^{1}Se-*-^{2}Se	0.0231	0.0041	−0.0012	0.0042	106.8	15.96	161.2	155	*r*-CS/CT-MC
^{2}Se-*-^{3}Se	0.0235	0.0046	−0.0014	0.0048	106.7	9.37	166.8	133	*r*-CS/CT-MC
^{3}Se-*-^{4}Se	0.0172	0.0037	−0.0002	0.0037	92.7	11.94	140.4	457	*r*-CS/*t*-HB$_{wc}$
^{4}Se-*-^{5}Se	0.0168	0.0043	0.0000	0.0043	90.5	5.09	130.5	400	*r*-CS/*t*-HB$_{wc}$
6^{2+}									
^{1}Se-*-^{1}'Se	0.0120	0.0030	0.0004	0.0031	82.6	16.45	107.7	373	*p*-CS/*t*-HB$_{nc}$
^{1}Se-*-^{2}Se	0.0164	0.0042	0.0000	0.0042	90.2	4.19	131.6	475	*r*-CS/*t*-HB$_{wc}$
^{2}Se-*-^{3}Se	0.0156	0.0035	0.0001	0.0035	89.2	8.68	129.1	538	*p*-CS/*t*-HB$_{nc}$
^{3}Se-*-^{4}Se	0.0217	0.0046	−0.0010	0.0047	102.1	5.99	155.8	196	*r*-CS/CT-MC
^{4}Se-*-^{5}Se	0.0187	0.0038	−0.0004	0.0038	95.8	11.56	144.1	321	*r*-CS/*t*-HB$_{wc}$
^{5}Se-*-^{6}Se	0.0176	0.0043	−0.0002	0.0043	92.4	5.01	135.2	332	*r*-CS/*t*-HB$_{wc}$
7^{2+}									
^{1}Se-*-^{1}'Se	0.0149	0.0041	0.0002	0.0041	87.1	4.96	121.1	461	*p*-CS/*t*-HB$_{nc}$
^{1}Se-*-^{2}Se	0.0107	0.0028	0.0005	0.0028	80.5	23.12	101.2	429	*p*-CS/*t*-HB$_{nc}$
^{2}Se-*-^{3}Se	0.0164	0.0043	0.0000	0.0043	90.1	4.58	131.6	468	*r*-CS/*t*-HB$_{wc}$
^{3}Se-*-^{4}Se	0.0150	0.0035	0.0001	0.0035	87.9	9.87	124.9	519	*p*-CS/*t*-HB$_{nc}$
^{4}Se-*-^{5}Se	0.0201	0.0045	−0.0006	0.0046	98.2	5.12	149.7	256	*r*-CS/*t*-HB$_{wc}$
^{5}Se-*-^{6}Se	0.0170	0.0037	−0.0001	0.0037	92.0	8.83	135.7	454	*r*-CS/*t*-HB$_{wc}$
^{6}Se-*-^{7}Se	0.0174	0.0044	−0.0001	0.0044	91.6	4.45	132.9	354	*r*-CS/*t*-HB$_{wc}$
8^{2+}									
^{1}Se-*-^{1}'Se	0.0102	0.0027	0.0005	0.0028	79.6	24.16	98.2	395	*p*-CS/*t*-HB$_{nc}$
^{1}Se-*-^{2}Se	0.0148	0.0041	0.0002	0.0041	87.0	3.98	120.4	443	*p*-CS/*t*-HB$_{nc}$
^{2}Se-*-^{3}Se	0.0113	0.0029	0.0004	0.0030	81.4	19.50	104.1	355	*p*-CS/*t*-HB$_{nc}$
^{3}Se-*-^{4}Se	0.0162	0.0042	0.0000	0.0042	89.7	4.06	129.6	459	*p*-CS/*t*-HB$_{nc}$
^{4}Se-*-^{5}Se	0.0145	0.0034	0.0002	0.0034	87.0	11.53	121.7	455	*p*-CS/*t*-HB$_{nc}$
^{5}Se-*-^{6}Se	0.0187	0.0044	−0.0004	0.0044	95.2	5.20	143.0	311	*r*-CS/*t*-HB$_{wc}$
^{6}Se-*-^{7}Se	0.0156	0.0036	0.0001	0.0036	89.0	7.47	126.6	477	*p*-CS/*t*-HB$_{nc}$
^{7}Se-*-^{8}Se	0.0163	0.0042	0.0000	0.0042	89.6	4.10	126.9	383	*p*-CS/*t*-HB$_{nc}$
1^{2+}									
^{1}Se-*-^{1}'Se	0.0964	-0.0051	−0.0386	0.0390	187.5	0.56	191.8	0.9	SS/Cov-w
2^{2+}									
^{1}Se-*-^{1}'Se	0.0642	0.0015	−0.0170	0.0171	175.1	1.49	190.2	7.5	*r*-CS/CT-TBP[i]
^{1}Se-*-^{2}Se	0.0411	0.0048	−0.0067	0.0082	144.2	2.18	177.7	42.4	*r*-CS/CT-MC
1									
^{1}Se-*-^{1}'Se	0.0114	0.0035	0.0006	0.0035	81.0	4.32	100.6	166	*p*-CS/*t*-HB$_{nc}$

[a] Calculated with M06-2X/BSS-A. [b] Data are given at BCPs. [c] $c\nabla^2\rho_b(r_c) = H_b(r_c) − V_b(r_c)/2$, where $c = \hbar^2/8\,m$. [d] $R = (x^2 + y^2)^{1/2}$, where $(x, y) = (H_b(r_c) − V_b(r_c)/2, H_b(r_c))$. [e] $\theta = 90° − \tan^{-1}(y/x)$. [f] Defined in eq (R1) of the references. [g] $\theta_p = 90° − \tan^{-1}(dy/dx)$. [h] $\kappa_p = |d^2y/dx^2|/[1 + (dy/dx)^2]^{3/2}$. [i] The borderline between the *r*-CS/CT-TBP nature and the SS/Cov-w nature.

interactions.[34a,35–38] The CS interactions are subdivided into $45° < \theta < 90°$ ($H_b(r_c) > 0$) for the *pure* CS interactions (*p*-CS) and $90° < \theta < 180°$ ($H_b(r_c) < 0$) for the *regular* CS interactions (*r*-CS). In the *p*-CS region of $45° < \theta < 90°$, the character of the interactions will be the vdW type for $45° < \theta_p < 90°$ ($45° < \theta < 75°$), whereas the character of the interactions will be the typical hydrogen bond type (*t*-HB) with no covalency (*t*-HB$_{nc}$) for $90° < \theta_p < 125°$ ($75° < \theta < 90°$), where $\theta = 75°$ and $\theta_p = 125°$ are tentatively given for $\theta_p = 90°$ and $\theta = 90°$, respectively. The CT interaction will appear in the *r*-CS region of $90° < \theta < 180°$. The *t*-HB interactions with covalency (*t*-HB$_{wc}$) appear in the range of $125° < \theta_p < 150°$ ($90° < \theta < 115°$), where $(\theta, \theta_p) = (115°, 150°)$ is tentatively given as the borderline between the *t*-HB$_{wc}$ and CT-

MC (molecular complex formation through CT) nature. The borderline between CT-MC and CT-TBP (TBP adduct formation through CT) types of the interactions is defined by $\theta_p = 180°$ ($\theta = 150°$), where $\theta = 150°$ is tentatively given, corresponding to $\theta_p = 180°$. The borderline between CT-TBP and Cov-w (weak covalent bonds) is defined by $\theta = 180°$ ($\theta_p = 190°$), where $\theta_p = 190°$ is tentatively given, corresponding to $\theta = 180°$. As a result, the (θ, θ_p) values of $(75°, \mathbf{90°})$, $(\mathbf{90°}, 125°)$, $(115°, \mathbf{150°})$, $(150°, \mathbf{180°})$, and $(\mathbf{180°}, 190°)$ correspond to the borderlines between the nature of interactions for vdW/*t*-HB$_{nc}$, *t*-HB$_{nc}$/*t*-HB$_{wc}$, *t*-HB$_{wc}$/CT-MC, CT-MC/CT-TBP, and CT-TBP/Cov-w, respectively. The parameters, described in bold, are superior to those tentatively given parameters in the classification and/or characterization of

ChemistryOpen

Full Papers
doi.org/10.1002/open.202100017

Chemistry Europe
European Chemical
Societies Publishing

interactions. The strong covalent bonds (Cov-s) of SS ($180° < \theta$) are not detected in this work, since R in Table 1 are smaller than 0.05 au (< 0.15 au), where the borderline between Cov-w and Cov-s is defined by $R = 0.15$ au. Consequently, the nature of each Se-*-Se in Table 1 can be classified and characterized based on the (θ, θ_p) values.

Each Se-*-Se interaction of 3^{2+}–8^{2+} in Table 1 is now classified and characterized based on the (θ, θ_p) values, evaluated with M06-2X/BSS-A, employing the QTAIM-DFA parameters of the standard interactions as a reference. Before discussion of Se-*-Se in 3^{2+}–8^{2+}, the nature of Se-*-Se in **1**, **1**$^{2+}$ and **2**$^{2+}$, are surveyed, as the starting points. The (θ, θ_p) values for ^{1}Se-*-$^{1'}$Se in **1** are (81.0°, 100.6°). Therefore, the interaction is classified by the p-CS interaction and characterized to have the t-HB$_{nc}$ nature, which is denoted by p-CS/t-HB$_{nc}$. However, the (θ, θ_p) values are (187.5°, 191.8°) for ^{1}Se-*-$^{1'}$Se in **1**$^{2+}$; therefore, it is classified by the SS interaction and characterized as the Cov-w nature (SS/Cov-w). The results show that the weak σ(2c–4e) interaction of p-CS/t-HB$_{nc}$ for ^{1}Se-*-$^{1'}$Se in **1** becomes the strong σ(2c–2e) interaction of SS/Cov-w in **1**$^{2+}$, through the removal of two electrons from the σ*(^{1}Se-*-$^{1'}$Se) orbital. The ^{1}Se-*-$^{1'}$Se, ^{1}Se-*-^{2}Se, and $^{1'}$Se-*-^{2}Se interactions in **2**$^{2+}$ construct σ(4c–6e). The (θ, θ_p) values for ^{1}Se-*-$^{1'}$Se and ^{1}Se-*-^{2}Se are (175.1°, 190.2°) and (144.2°, 177.7°), respectively. Therefore, the ^{1}Se-*-$^{1'}$Se and ^{1}Se-*-^{2}Se interactions are predicted to have the r-CS/CT-TBP and r-CS/CT-MC natures, respectively.

The QTAIM-DFA parameters for ^{1}Se-*-$^{1'}$Se in **1** and **1**$^{2+}$ evaluated with MP2/BSS-B and for ^{1}Se-*-$^{1'}$Se and ^{1}Se-*-^{2}Se in **2**$^{2+}$ evaluated with M06-2X/BSS-B are collected in Table S4 of the Supporting Information, together with the QTAIM functions and the predicted nature. The predicted nature for each interaction with M06-2X/BSS-A is the same as that corresponding interaction in **1** and **1**$^{2+}$ with MP2/BSS-B and in **2**$^{2+}$ with M06-2X/BSS-B, although there are some differences in the calculated parameters. Consequently, the small differences between the QTAIM-DFA parameters calculated with M06-2X/BSS-A and those obtained with MP2/BSS-B and M06-2X/BSS-B are confirmed not to damage our discussion so much on the nature of the interactions. The nature of each Se-*-Se in 3^{2+}–8^{2+}, together with **1**$^{2+}$ and **2**$^{2+}$, will be discussed based on the parameters evaluated with M06-2X/BSS-A, which enables us to discuss the nature of Se-*-Se in **1**$^{2+}$–8^{2+}, in a unified form.

Each Se-*-Se interaction in 3^{2+}–8^{2+} is expected to have a nature between that of **1** and **1**$^{2+}$. The (θ, θ_p) values for ^{1}Se-*-$^{1'}$Se of 3^{2+} are (159.7°, 183.4°), therefore, it is predicted to have the r-CS/CT-TBP nature. The values for ^{1}Se-*-^{2}Se and ^{2}Se-*-^{3}Se of 3^{2+} are (101.9–141.0°, 151.9–177.1°), therefore, they are predicted to have the r-CS/CT-MC nature. In the case of 4^{2+}, the (θ, θ_p) values for ^{1}Se-*-$^{1'}$Se, ^{1}Se-*-^{2}Se, and ^{2}Se-*-^{3}Se are (103.5–142.0°, 153.6–178.8°), which are predicted to have the r-CS/CT-MC nature. The values for ^{3}Se-*-^{4}Se are (90.0°, 128.4°), therefore, it is just on the borderline area between p-CS/t-HB$_{nc}$ and r-CS/t-HB$_{wc}$. The (θ, θ_p) values for ^{1}Se-*-$^{1'}$Se, ^{1}Se-*-^{2}Se, and ^{2}Se-*-^{3}Se of 5^{2+} are (106.7–114.1°, 161.2–170.2°), therefore, they are predicted to have the r-CS/CT-MC nature. The values for ^{3}Se-*-^{4}Se and ^{4}Se-*-^{5}Se are (90.5–92.7°, 130.5–140.4°), and they are predicted to have the r-CS/t-HB$_{wc}$ nature, although ^{3}Se-*-^{4}Se

seems close to the borderline area between p-CS/t-HB$_{nc}$ and r-CS/t-HB$_{wc}$.

In the case of 6^{2+}, while the (θ, θ_p) values for ^{1}Se-*-$^{1'}$Se and ^{2}Se-*-^{3}Se are (82.6–89.2°, 107.7–129.1°), which are predicted to have the p-CS/t-HB$_{nc}$ nature, the values for ^{1}Se-*-^{2}Se, ^{4}Se-*-^{5}Se, and ^{5}Se-*-^{6}Se are (90.2–95.8°, 131.6–144.1°), which are predicted to have the r-CS/t-HB$_{wc}$ nature. The (θ, θ_p) values for ^{3}Se-*-^{4}Se are (102.1°, 155.8°), which is predicted to have the r-CS/CT-MC nature. Similar to the case of 6^{2+}, the (θ, θ_p) values for ^{1}Se-*-$^{1'}$Se, ^{1}Se-*-^{2}Se, and ^{3}Se-*-^{4}Se of 7^{2+} are (80.5–87.9°, 101.2–124.9°), which are predicted to have the p-CS/t-HB$_{nc}$ nature, whereas the (θ, θ_p) values for ^{2}Se-*-^{3}Se, ^{4}Se-*-^{5}Se, ^{5}Se-*-^{6}Se, and ^{6}Se-*-^{7}Se are (90.1–98.2°, 131.6–149.7°), which are predicted to have the r-CS/t-HB$_{wc}$ nature. However, ^{2}Se-*-^{3}Se ($\theta = 90.1$°) is very close to the borderline area to the p-CS/t-HB$_{nc}$ nature, and ^{4}Se-*-^{5}Se ($\theta_p = 149.7$°) is close to the borderline area for the p-CS/CT-MC nature. Contrary to the cases of 6^{2+} and 7^{2+}, the Se-*-Se interactions of 8^{2+} are all predicted to have the p-CS/t-HB$_{nc}$ nature by the (θ, θ_p) values of (79.6–89.7°, 98.2–129.6°), except for ^{5}Se-*-^{6}Se with (θ, θ_p) = (95.2°, 143.0°), which is predicted to have the nature of p-CS/t-HB$_{wc}$, although ^{3}Se-*-^{4}Se and ^{7}Se-*-^{8}Se seem close to the borderline area for the r-CS/t-HB$_{wc}$ nature with (θ, θ_p) = (89.6–89.7°, 126.9–129.6°).

Weak interactions of the Se-H and H–H types are also observed between the components in 6^{2+}–8^{2+}, which are analyzed similarly. The results are shown in Table S5 of the Supporting Information. The interactions are all predicted to have the p-CS/vdW nature.

2.5. Relations Between QTAIM-DFA Parameters and C_{ii}

What are the relations among the QTAIM-DFA parameters? Before the discussion, the parameters of R, θ, and θ_p are plotted versus $\rho(r)$, which are shown in Figure S4 of the Supporting Information. The parameters increase monotonically as the increase of $\rho(r)$, although the plots are convex downward for R and convex upward for θ and θ_p. The plot for R versus $\rho(r)$ would be imaged as two streams. Then, θ and θ_p are plotted versus R, separately by the Se-*-Se interactions inside or outside Se(CH$_2$CH$_2$CH$_2$)$_2$Se in 3^{2+}–8^{2+}, together with **1**, **1**$^{2+}$ and **2**$^{2+}$. Figure 8 shows the plot, which reveals the two streams of the data (points) for R, θ, and θ_p, (see also Figure 4). The results show that the (CH$_2$CH$_2$CH$_2$)$_2$ chains between the Se atoms in Se(CH$_2$CH$_2$CH$_2$)$_2$Se of **1**$^{2+}$–8^{2+} and **1** affect the parameters depending on the inside or outside positions of the components. However, the magnitudes in the differences of the parameters are very small. As a result, σ($m_c c$-$n_e e$: $4 \leq m_c \leq 16$) formed in 3^{2+}–8^{2+} and **2**$^{2+}$ seem not to be affected so much from the chain. Namely, the σ-type linear Se$_{2n}$ interactions in **2**$^{2+}$–8^{2+} would be close to those formed without any restrictions.

The R values are next plotted versus $1/C_{ii}$ for all Se-*-Se in 3^{2+}–8^{2+}, together with **1**$^{2+}$ and **2**$^{2+}$. The plot, shown in Figure S5 of the Supporting Information, gave a good correlation ($R = 0.0207(1/C_{ii}) + 0.0009$: $R_c^2 = 0.956$). The results show that the strength of Se-*-Se can be estimated not only by R but
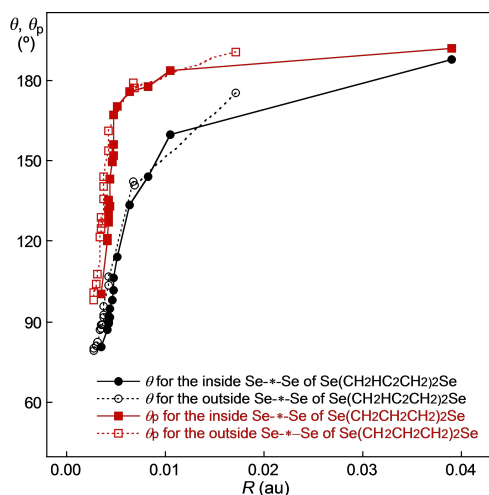
ChemistryOpen

Full Papers
doi.org/10.1002/open.202100017

Chemistry Europe
European Chemical
Societies Publishing

Figure 8. Plots of θ and θ_p versus R for Se-*-Se in 1^{2+}–8^{2+} and **1**.

also by $1/C_{ii}$, although roughly. The θ values show similar correlation to $1/C_{ii}$, although the data from Se-*-Se in 1^{2+} deviate from the correlation. The correlation between θ_p and $1/C_{ii}$ seems poor. The $\rho_b(r_c)$ values also show good correlation to $1/C_{ii}$, although the data from Se-*-Se in 1^{2+} deviate from the correlation, similar to the case of θ.

2.6. NBO Analysis for each Se-*-Se Interaction in 1^{2+}–8^{2+}

How does the CT term of each Se-*-Se contribute to stabilize 3^{2+}–8^{2+} and 2^{2+}? The second-order perturbation energies of $E(2)$ are examined for the n(Se)→σ*(Se-Se) 3c–4e type interactions in 2^{2+}–8^{2+} by the NBO analysis.[33]

The CT contributions in the intramolecular n(Se)→σ*(Se-Se) interactions of 3^{2+}–8^{2+} and 2^{2+} seem very different from the typical cases. The linear Se_{2n} interactions of 3^{2+}–8^{2+} and 2^{2+} construct the conjugate system of the σ-type, and the SeSeSe angles of the interactions are often smaller than 150°, which we proposed tentatively as a lower limit for the linear interactions. The positive charge on the species would accelerate the mixing of the orbitals between those on Se and the frameworks constructed by C and H. There seem to be many candidates for the CT interactions in the linear Se_{2n} interactions of 2^{2+}–8^{2+}. However, such CT terms were detected for the typical cases in 3^{2+}–5^{2+} and 7^{2+} (and 2^{2+}) but not in 6^{2+} and 8^{2+}. It would be difficult to specify the n(Se)→σ*(Se-Se) 3c–4e type interactions among many candidates in the linear σ-type Se_{2n} interactions of 2^{2+}–8^{2+}. The detection of the non-adjacent n(Se)→σ*(Se-Se) 3c–4e type interactions, such as $n_p(^3Se)$→σ*(^1Se-$^1'Se$) in 3^{2+}–5^{2+} and $n_p(^3Se)$→σ*(^5Se-^6Se) and $n_p(^2Se)$→σ*(^5Se-^6Se) in 5^{2+} must also be derived from the conjugated linear σ-type Se_{2n} interactions of 2^{2+}–8^{2+}. Detected $E(2)$ values for 2^{2+}–5^{2+} and 7^{2+}, are collected in Table S6 of the Supporting Information, where only one side of the interactions is considered for the symmetric species. Large $E(2)$ values are predicted for n_p-(Se)→σ*(Se-Se) 3c–4e, which is consistent for the interactions being formed in the conjugated linear σ-type Se_{2n} interactions.

Only fairly good correlations were obtained between $E(2)$ and $1/C_{ii}$, irrespective of other cases. The results show that the energies for the conjugated linear σ-type Se_{2n} interactions of 3^{2+}–8^{2+} and 2^{2+} cannot be fractionalized well to each evaluated by $1/C_{ii}$, namely the interactions in 3^{2+}–8^{2+} should be analyzed as σ(m_cc-n_ee: $6 \leq m_c \leq 16$).

3. Conclusions

The nature of the extended hypervalent interactions of σ(m_cc-n_ee: $m_c \geq 6$) has been investigated. Such interactions are elucidated for 3^{2+}–8^{2+}, together with 2^{2+}. The magnitudes of ΔE in the formation of n^{2+} from $[1^{2+} + (n-1) \cdot 1]$ ($n = 2$–8) are shown to increase almost constantly by approximately 0.38 eV. The $r(^uSe, ^vSe)$ values must be closely related to the stability of the dicationic oligomers (ΔE), which correlate well with (Qn-(^uSe) + $Qn(^vSe)$) for 3^{2+}–8^{2+}, together with **1**, 1^{2+}, and 2^{2+}. Very good correlations are obtained, if analyzed as two correlations, although the data of 1^{2+} are omitted. The results strongly suggest that the Se-Se interactions will be stronger than the electrostatic repulsion of the positive charges developed at both sides of Se-Se in 3^{2+}–8^{2+}, together with **1**, 1^{2+}, and 2^{2+}. The electrostatic terms can be estimated by $Qn(^uSe) + Qn(^vSe)$, which must also correlate with the contributions of Se_2 σ(2c–2e).

QTAIM-DFA with CIV is applied to elucidate the intrinsic dynamic and static nature of the Se-*-Se interactions in 1^{2+}–8^{2+} with **1**, after clarification of the structural feature. The nature of the Se-*-Se interactions in 1^{2+}–8^{2+} with **1** is summarized as follows. The ^uSe-*-^vSe interaction in the same species becomes weaker if it goes from the central position to a more outside position for 2^{2+}–5^{2+}, although the order changes as in ^2Se-*-^3Se > ^1Se-*-^2Se for 5^{2+}. However, ^1Se-*-$^1'Se$ is weakest in 6^{2+} and 8^{2+}, while ^1Se-*-^2Se is weakest in 7^{2+}. The strength of ^uSe-*-^vSe shows ripple-like changes from the central to the outside for 6^{2+}–8^{2+}. The predicted nature of each Se-*-Se in 1^{2+}–8^{2+} is summarized in Table 1. The nature of Se-*-Se predicted by the QTAIM parameters should be closely related to that in $r(Se, Se)$, as a whole. The $(CH_2CH_2CH_2)_2$ chains in 1^{2+}–8^{2+} and **1** affect the QTAIM-DFA parameters, although slightly. Therefore, σ(m_cc-n_ee: $4 \leq m_c \leq 16$) formed in 2^{2+}–8^{2+} should be close to those formed without any limitations. The strength of Se-*-Se described by R can be estimated by $1/C_{ii}$. The $E(2)$ values based on NBO revealed the specific behavior of the conjugated σ-type Se_n^{2+} interactions in 2^{2+}–8^{2+}. The results show that the linear Se_n^{2+} interactions of $6 \leq n \leq 16$ should be analyzed as σ(m_cc-n_ee: $6 \leq m_c \leq 16$), not by the accumulated σ(3c–4e).

Indeed, 3^{2+}–8^{2+} are demonstrated to be energetically stable, similarly to the case of 2^{2+}, however, 3^{2+}–8^{2+} are not isolated, yet. The entropy term must play an important role under the experimental conditions, in addition to the enthalpy term. The entropy term contributes much to isolate 1^{2+} and 2^{2+}. The term will work more negatively as n in n^{2+} becomes larger. As a result, the next target to isolate n^{2+} should be $n = 3$, if the entropy term is considered. But n^{2+} ($n > 3$) could be isolated, if the specific stabilization conditions, such as those

from the crystal packing effect and/or the counter ions, are satisfied.

Conflict of Interest

The authors declare no conflict of interest.

[1] a) W. Nakanishi, S. Hayashi, S. Toyota, *Chem. Commun.* **1996**, 371–372; W. Nakanishi, S. Hayashi, S. Toyota, *J. Org. Chem.* **1998**, *63*, 8790–8800; b) W. Nakanishi, S. Hayashi, T. Arai, *Chem. Commun.* **2002**, 2416–2417; c) W. Nakanishi, S. Hayashi, S. Morinaka, T. Sasamori, N. Tokitoh, *New J. Chem.* **2008**, *32*, 1881–1889; d) W. Nakanishi, S. Hayashi, N. Itoh, *Chem. Commun.* **2003**, 124–125; W. Nakanishi, S. Hayashi, N. Itoh, *J. Org. Chem.* **2004**, *69*, 1676–1684.

[2] a) W. Nakanishi, *Hypervalent Chalcogen Compounds in Handbook of Chalcogen Chemistry: New Perspectives in Sulfur, Selenium and Tellurium* (Ed.: F. A. Devillanova), Royal Society of Chemistry, Cambridge, **2006**, Chap. 10.3, pp 644–668; b) W. Nakanishi, S. Hayashi, *Hypervalent Chalcogen Compounds In Handbook of Chalcogen Chemistry: New Perspectives in Sulfur, Selenium and Tellurium*: 2nd Edition, Vol. 2, (Eds.: F. A. Devillanova, W.-W. du Mont), Royal Society of Chemistry, Cambridge, **2013**, Chap. 12.3, pp 335–372; c) *The Chemistry of Organic Selenium and Tellurium Compounds* (Eds.: S. Patai, Z. Rappoport), John-Wiley and Sons, New York, **1986**, Vols. 1 and 2.

[3] A. J. Mukherjee, S. S. Zade, H. B. Singh, R. B. Sunoj, *Chem. Rev.* **2010**, *110*, 4357–4416.

[4] *Chemistry of Hypervalent Compounds* (Ed.: K.-Y. Akiba), Wiley-VCH, New York, **1999**.

[5] Y. Tsubomoto, S. Hayashi, W. Nakanishi, T. Sasamori, N. Tokitoh, *Acta Crystallogr.* **2017**, *B73*, 265–275.

[6] a) W. Nakanishi, S. Hayashi, S. Yamaguchi, K. Tamao, *Chem. Commun.* **2004**, 140–141; b) P. C. Srivastava, S. Bajpai, S. Bajpai, C. Ram, R. Kumar, J. P. Jasinski, R. J. Butcher, *J. Organomet. Chem.* **2004**, *689*, 194–202; c) S. Hayashi, T. Nishide, W. Nakanishi, *Heteroat. Chem.* **2018**, e21462-1–12; d) S. Hayashi, T. Nishide, W. Nakanishi, *Bioinorg. Chem. Appl.* **2020**, 2901439-1–14.

[7] a) A. Panda, G. Mugesh, H. B. Singh, R. J. Butcher, *Organometallics* **1999**, *18*, 1986–1993; b) M. Kulcsar, A. Beleaga, C. Silvestru, A. Nicolescu, C. Deleanu, C. Todasca, A. Silvestru, *Dalton Trans.* **2007**, 2187–2196; c) A. Beleaga, M. Kulcsar, C. Deleanu, A. Nicolescu, C. Silvestru, A. Silvestru, *J. Organomet. Chem.* **2009**, *694*, 1308–1316.

[8] See also W. Nakanishi, T. Nakamoto, S. Hayashi, T. Sasamori, N. Tokitoh, *Chem. Eur. J.* **2007**, *13*, 255–268.

[9] a) H. Fujihara, T. Nakahodo, N. Furukawa, *Chem. Commun.* **1996**, 311–312; b) H. Fujihara, H. Ishitani, Y. Takaguchi, N. Furukawa, *Chem. Lett.* **1995**, 571–572; c) N. Furukawa, T. Fujii, T. Kimura, H. Fujihara, *Chem. Lett.* **1994**, 1007–1010; d) H. Fujihara, R. Saito, M. Yabe, N. Furukawa, *Chem. Lett.* **1992**, 1437–1440; e) H. Fujihara, M. Yabe, J.-J. Chiu, N. Furukawa, *Tetrahedron Lett.* **1991**, *32*, 4345–4348.

[10] R. S. Glass, L. Adamowicz, J. L. Broeker, *J. Am. Chem. Soc.* **1991**, *113*, 1065–1072; R. S. Glass, S. W. Andruski, J. L. Broeker, H. Firouzabadi, L. K. Steffen, G. S. Wilson, *J. Am. Chem. Soc.* **1989**, *111*, 4036–4045.

[11] a) A. Wakamiya, T. Nishinaga, K. Komatsu, *J. Am. Chem. Soc.* **2002**, *124*, 15038–15050. See also; b) K. Morihashi, S. Kushihara, Y. Inadomi, O. Kikuchi, *J. Mol. Struct. (Theochem)* **1997**, *418*, 171–178; c) B. Mueller, T. T. Takaluoma, R. S. Laitinen, K. Seppelt, *Eur. J. Inorg. Chem.* **2011**, 4970–

4977; d) B. Mueller, H. Poleschner, K. Seppelt, *Dalton Trans.* **2008**, 4424–4427.

[12] a) F. Iwasaki, N. Toyoda, R. Akaishi, H. Fujihara, N. Furukawat, *Bull. Chem. Soc. Jpn.* **1988**, *61*, 2563–2567; b) H. Fujihara, A. Kawada, N. Furukawa, *J. Org. Chem.* **1987**, *52*, 4254–4257.

[13] D. H. Evans, N. E. Gruhn, J. Jin, B. Li, E. Lorance, N. Okumura, N. A. Macias-Ruvalcaba, U. I. Zakai, S.-Z. Zhang, E. Block, R. S. Glass, *J. Org. Chem.* **2010**, *75*, 1997–2009.

[14] a) F. Iwasaki, M. Morimoto, M. Yasui, R. Akaishi, H. Fujihara, N. Furukawa, *Acta Crystallogr. Sect. C* **1991**, *C47*, 1463–1466; b) H. Fujihara, N. Furukawa, *Phosphorus Sulfur Silicon Relat. Elem.* **1992**, *67*, 131–134.

[15] D. H. Evans, N. E. Gruhn, J. Jin, B. Li, E. Lorance, N. Okumura, N. A. Macias-Ruvalcaba, U. I. Zakai, S.-Z. Zhang, E. Block, R. S. Glass, *J. Org. Chem.* **2010**, *75*, 1997–2009.

[16] K. George, M. Jura, W. Levason, M. E. Light, L. P. Ollivere, G. Reid, *Inorg. Chem.* **2012**, *51*, 2231–2240.

[17] In the Cambridge Structural Database (CSD), the neutral species **1** has been characterized in its Ag(I) and Pd(II) complexes (NOWKOZ[36] and ZATMEM,[37] respectively) and the adduct with GaCl₃ (CAXJUI),[16] SbCl₃ (EWIWAI),[38] MnBr(CO)₃ (FAWQEZ),[39] ReBr(CO)₃ (FAWQID),[39] and W(CO)₄ (FAWQOJ),[39] together with the tetramethyl derivative (RIYSIB01).[40] The dimer **2**²⁺ was deposited as CAXKET,[16] while **1**²⁺ was reported as solvate tetrafluoroborate salt (KIVHIG).[14a] The chloro-derivative of **1** shows an Se···Se intermolecular distance of 3.773 Å in its GaCl₄⁻ solvate salt (CAXKIX)[16] and the hydroxo-derivative an Se···Se intermolecular distance of 3.499 Å in its copper complex (MELSOL).[41] No example of Se···(Se-Se)···Se could be found within the sum of vdW radii, other than above.

[18] a) S. Hayashi, K. Nagata, S. Otsuki, W. Nakanishi, *J. Phys. Chem. A* **2017**, *121*, 2482–2496; b) S. Hayashi, K. Matsuiwa, N. Nishizawa, W. Nakanishi, *J. Org. Chem.* **2015**, *80*, 11963–11976.

[19] a) W. Nakanishi, S. Hayashi, K. Narahara, *J. Phys. Chem. A* **2009**, *113*, 10050–10057; b) W. Nakanishi, S. Hayashi, *Curr. Org. Chem.* **2010**, *14*, 181–197; c) W. Nakanishi, S. Hayashi, *J. Phys. Chem. A* **2010**, *114*, 7423–7430; d) W. Nakanishi, S. Hayashi, K. Matsuiwa, M. Kitamoto, *Bull. Chem. Soc. Jpn.* **2012**, *85*, 1293–1305; e) W. Nakanishi, S. Hayashi, *J. Phys. Chem. A* **2013**, *117*, 1795–1803.

[20] a) *Atoms in Molecules. A Quantum Theory*, (Ed.: R F. W. Bader), Oxford University Press, Oxford, UK, **1990**; b) C. F. Matta, R. J. Boyd, *An Introduction to the Quantum Theory of Atoms in Molecules in The Quantum Theory of Atoms in Molecules: From Solid State to DNA and Drug Design* (Eds.: C. F. Matta, R. J. Boyd), WILEY-VCH, Weinheim, Germany, **2007**, Chap. 1.

[21] The θ_p and κ_p for the major bonds seem to be controlled by the characters of the local bonds in question: The influence from the behaviors of the minor bonds would not be so severe for usual cases.

[22] W. Nakanishi, S. Hayashi, *Int. J. Quantum Chem.* **2018**, *118*, e25590-1–14.

[23] The basic concept for the compliance constants was introduced by Taylor and Pitzer,[42] followed by Konkoli and Cremer.[43]

[24] The C_{ij} are defined as the partial second derivatives of the potential energy due to an external force, as shown in eq (R1),[44,45] where i and j refer to internal coordinates, and the external force components acting on the system f_i and f_j correspond to i and j, respectively. $C_{ij} = \partial^2 E / \partial f_i \partial f_j$ (R1) The C_{ij} values and the coordinates corresponding to C_{ii} were calculated by using the Compliance 3.0.2 program released by J. Grunenberg and K. Brandhorst, http://www.oc.tu-bs.de/Grunenberg/compliance.html.

[25] a) K. Brandhorst, J. Grunenberg, *J. Chem. Phys.* **2010**, *132*, 184101-1–7; b) K. Brandhorst, J. Grunenberg, *Chem. Soc. Rev.* **2008**, *37*, 1558–1567; c) J. Grunenberg, *Chem. Sci.* **2015**, *6*, 4086–4088.

[26] a) J. Grunenberg, *J. Am. Chem. Soc.* **2004**, *126*, 16310–16311, see also; b) J. Grunenberg, G. Barone, *RSC Adv.* **2013**, *3*, 4757–4762.

[27] *The Chemistry of Organic Selenium and Tellurium Compounds* (Ed. Z. Rappoport) Wiley, New York, **2013**, Chaps. 11, 13–16, Vol. 4, pp. 885–972 and pp. 989–1236.

[28] a) Y. Tsubomoto, S. Hayashi, W. Nakanishi, L. K. Mapp, S. J. Coles, *RSC Adv.* **2018**, *8*, 9651–9660; b) W. Nakanishi, Y. Tsubomoto, S. Hayashi, *RSC Adv.* **2016**, *6*, 93195–93204.

[29] a) M. C. Durrant, *Chem. Sci.* **2015**, *6*, 6614–6623; b) M. S. Schmøkel, S. Cenedese, J. Overgaard, M. R. V. Jørgensen, Y.-S. Chen, C. Gatti, D. Stalke, B. B. Iversen, *Inorg. Chem.* **2012**, *51*, 8607–8616.

[30] M. J. Frisch, G. W. Trucks, H. B. Schlegel, G. E. Scuseria, M. A. Robb, J. R. Cheeseman, G. Scalmani, V. Barone, B. Mennucci, G. A. Petersson, H. Nakatsuji, M. Caricato, X. Li, H. P. Hratchian, A. F. Izmaylov, J. Bloino, G. Zheng, J. L. Sonnenberg, M. Hada, M. Ehara, K. Toyota, R. Fukuda, J.

Hasegawa, M. Ishida, T. Nakajima, Y. Honda, O. Kitao, H. Nakai, T. Vreven, J. A. Montgomery, Jr., J. E. Peralta, F. Ogliaro, M. Bearpark, J. J. Heyd, E. Brothers, K. N. Kudin, V. N. Staroverov, R. Kobayashi, J. Normand, K. Raghavachari, A. Rendell, J. C. Burant, S. S. Iyengar, J. Tomasi, M. Cossi, N. Rega, J. M. Millam, M. Klene, J. E. Knox, J. B. Cross, V. Bakken, C. Adamo, J. Jaramillo, R. Gomperts, R. E. Stratmann, O. Yazyev, A. J. Austin, R. Cammi, C. Pomelli, J. W. Ochterski, R. L. Martin, K. Morokuma, V. G. Zakrzewski, G. A. Voth, P. Salvador, J. J. Dannenberg, S. Dapprich, A. D. Daniels,"O. Farkas, J. B. Foresman, J. V. Ortiz, J. Cioslowski, D. J. Fox, *Gaussian 09*, *Revision D.01*, Gaussian, Inc., Wallingford CT, **2009**.

[31] Y. Zhao, D. G. Truhlar, *Theor. Chem. Acc.* **2008**, *120*, 215–241.

[32] a) C. Møller, M. S. Plesset, *Phys. Rev.* **1934**, *46*, 618–622; b) J. Gauss, *J. Chem. Phys.* **1993**, *99*, 3629–3643; c) J. Gauss, *Ber. Bunsen-Ges. Phys. Chem.* **1995**, *99*, 1001–1008.

[33] The $E(2)$ stabilization energy of the NBO (i: donor)→NBO (j: acceptor) type is estimated according to eq (R2), where q_i is the donor orbital occupancy, E_i and E_j are the orbital energies of diagonal elements, and F(i, j) is the off-diagonal NBO Fock matrix element. $E(2) = q_i F(i, j)^2/(E_i - E_j)$ (R2)
See, E. D. Glendening, J. K. Badenhoop, A. E. Reed, J. E. Carpenter, J. A. Bohmann, C. M. Morales, C. R. Landis, F. Weinhold, NBO Version 6.0. **2013**.

[34] The AIM2000 program (Version 2.0) is employed to analyze and visualize atoms-in-molecules: F. Biegler-König, *J. Comput. Chem.* **2000**, *21*, 1040–1048.

[35] T. A. Keith, AIMAll (Version 17.11.14), TK Gristmill Software, Overland Park KS, USA, **2017**, http://www.aim.tkgristmill.com.

[36] D. G. Booth, W. Levason, J. J. Quirk, G. Reid, S. M. Smith, *J. Chem. Soc. Dalton Trans.* **1997**, 3493–3500.

[37] N. R. Champness, W. Levason, J. J. Quirk, G. Reid, C. S. Frampton, *Polyhedron* **1995**, *14*, 2753–2758.

[38] N. J. Hill, W. Levason, R. Patel, G. Reid, M. Webster, *Dalton Trans.* **2004**, 980–981.

[39] M. K. Davies, M. C. Durrant, W. Levason, G. Reid, R. L. Richards, *J. Chem. Soc. Dalton Trans.* **1999**,1077–1084.

[40] R. D. Adams, K. T. McBride, R. D. Rogers, *Organometallics* **1997**, *16*, 3895–3901.

[41] R. J. Batchelor, F. W. B. Einstein, I. D. Gay, J.-H. Gu, S. Mehta, B. M. Pinto, X.-M. Zhou, *Inorg. Chem.* **2000**, *39*, 2558–2571.

[42] W. T. Taylor, K. S. Pitzer, *J. Res. Natl. Bur. Stand.* **1947**, *38*, 1–17.

[43] Z. Konkoli, D. Cremer, *Int. J. Quantum Chem.* **1998**, *67*, 1–9.

[44] a) J. Grunenberg, N. Goldberg, *J. Am. Chem. Soc.* **2000**, *122*, 6045–6047; b) J. Grunenberg, R. Streubel, G. v. Frantzius, W. Marten, *J. Chem. Phys.* **2003**, *119*, 165–169.

[45] Y. Xie, H. F. I. Schaefer, *Z. Phys. Chem.* **2003**, *217*, 189–203.